

Linking uplift, erosion, and sedimentation using landscape evolution models: Madagascar since the Late Cretaceous

Ruohong Jiao^{1,2}  | Jean Braun¹ | Antoine Delaunay^{3,4} | Cécile Robin³ | François Guillocheau³

¹Helmholtz Centre Potsdam, GFZ German Research Centre for Geosciences, Potsdam, Germany

²School of Earth and Ocean Sciences, University of Victoria, Victoria, British Columbia

³Géosciences Rennes, Université de Rennes 1, Rennes, France

⁴Ali Al-Naimi Petroleum Engineering Research Center, King Abdullah University of Science and Technology, Thuwal, Saudi Arabia

Correspondence

Ruohong Jiao, School of Earth and Ocean Sciences, University of Victoria, Victoria, British Columbia V8P 5C2, Canada.
Email: rjiao@uvic.ca

Summary

We present a study to estimate the large-scale landscape history of a continental margin, by establishing a source-to-sink volume balance between the eroding onshore areas and the offshore basins. Assuming erosion as the primary process for sediment production, we strive to constrain a numerical model of landscape evolution that balances the volumes of eroded materials from the continent and that deposited in the corresponding basins, with a ratio imposed for loss of erosion products. We use this approach to investigate the landscape history of Madagascar since the Late Cretaceous. The uplift history prescribed in the model is inferred from elevations of planation surfaces formed at various ages. By fitting the volumes of terrigenous sediments in the Morondava Basin along the west coast and the current elevation of the island, the landscape evolution model is optimized by constraining the erosion law parameters and ratios of sediment loss. The results include a best-fit landscape evolution model, which features two major periods of uplift and erosion during the Late Cretaceous and the middle to late Cenozoic. The model supports suggestions from previous studies that most of the high topography of the island was constructed since the middle to late Miocene, and on the central plateau the erosion has not reached an equilibrium with the high uplift rates in the late Cenozoic. Our models also indicate that over the geological time scale a significant portion of materials eroded from Madagascar was not archived in the offshore basin, possibly consumed by chemical weathering, the intensity of which might have varied with climate.

KEYWORDS

chemical weathering, erosion, landscape evolution model, Madagascar, sedimentary basin, source to sink

1 | INTRODUCTION

The topography of a continent can be built by dynamic evolution of the Earth through processes such as plate convergence and mantle convection. On the other hand, the topographic relief is reduced by relocating or consuming rocks through erosion and weathering by physical, chemical, and biological activities. As the topography controls the routing of freshwater and sediment, atmospheric circulation patterns, and distribution and evolution of the biota, estimating the

landscape evolution of a region is valuable for understanding how these systems evolve and interact. Sediments accumulated in basins adjacent to uplifted areas can be used to provide information on the landscape history of the source regions. Paleoelevation and paleorelief can be estimated using isotope-based methods (e.g., Rowley & Garzzone, 2007; Zhuang et al., 2019), but these empirical methods are limited by the availability of samples in the stratigraphy. Changes in sedimentation rate are also used for inferring variations in erosion rate in the provenance (e.g., Zhang et al., 2001), to reflect

This is an open access article under the terms of the [Creative Commons Attribution-NonCommercial](https://creativecommons.org/licenses/by-nc/4.0/) License, which permits use, distribution and reproduction in any medium, provided the original work is properly cited and is not used for commercial purposes.

© 2022 The Authors. *Earth Surface Processes and Landforms* published by John Wiley & Sons Ltd.

modifications of the regional elevation or relief. However, sediment accumulation rates estimated from one-dimensional age–depth profiles are biased by the incomplete stratigraphy (Sadler, 1981), and therefore reliable estimates of the erosion rates of the source regions require stratigraphic records in two (across the basin margin) or three dimensions.

We demonstrate a case study in Madagascar, in which a numerical model of the landscape evolution is constrained using sediment volume data from basins on the continental margin. As a former part of Gondwana, Madagascar was separated from Africa at ~160 Ma, from Antarctica at ~120 Ma, and from the Seychelles and India at ~90 Ma (de Wit, 2003). Thereafter, since the Late Cretaceous, Madagascar as an island in the Indian Ocean has its own geological history on a passive margin. Recovering the landscape history of the island will help in understanding the interaction between the Earth's tectonic, mantle, and surface processes (Emmel et al., 2012; Roberts et al., 2012; Stephenson et al., 2021). This long-term isolation of the island from other continental masses resulted in a relatively closed system for its crustal material, which was redistributed by erosion, transport, and sedimentation processes following uplift of the island. If the input from magmatism (e.g., Storey et al., 1995) can be ignored and a closed system of sediment cycling can be assumed, the volume of siliciclastic sediments deposited in the basins should in general be equal to the total onshore erosion after subtracting the component consumed by weathering. This simple balance allows us to link the two using a landscape evolution model (LEM) which could be constrained by empirical data. Here, by using a formal inversion method—that is, the Neighbourhood Algorithm (Sambridge, 1999)—we attempt to optimize an LEM of Madagascar that reproduces volumetric sedimentary history in the basin. The results provide estimates of the erosion history of the island and portions of potential sediment loss, with implications about the factors that could affect erosion and weathering intensities in tectonically inactive regions.

2 | RESEARCH BACKGROUND AND DATA

2.1 | Uplift history of Madagascar

The landscape of present-day Madagascar has been built by significant rock uplift accumulated over a long history. The Mesozoic uplift and exhumation histories of Madagascar were recorded by low-temperature thermochronology. The oldest apatite fission-track (AFT) cooling ages are in the range of ~440–200 Ma, and occur on the central plateau to the south of the Cenozoic volcanoes (Itasy and Ankaratra; Figure 1b) (Emmel et al., 2006, 2008, 2012; Jöns et al., 2009; Seward et al., 2004; Stephenson et al., 2021). These ages indicate that since the Paleozoic the total exhumation of this part of the plateau was less than the closure depth of the AFT system (~4 km). During the Late Cretaceous, the final break-up between Madagascar and the Seychelles–India block was possibly triggered by the passage of the Marion hot spot (Storey et al., 1995; Torsvik et al., 1998). Mantle upwelling at the hot spot could have elevated the southeast of the island and tilted the island towards the northwest. Compared to the central plateau, AFT ages are younger (~119–68 Ma) along the east escarpment, but it is unclear whether these ages were thermally reset by the heat from the plume, or they reflect erosion of the uplifted rifting shoulder (Seward et al., 2004). Apatite (U–Th)/He cooling ages <60 Ma are also found on the coastal plain at the foot of the escarpment along the east coast of the island (Emmel et al., 2012), suggesting a possible retreat of the escarpment following the island's rifting from India.

The uplift history of Madagascar during the Cenozoic was constrained by the current elevations of the carbonate platforms and geometries of river long profiles. Shallow marine Eocene sediments occur in some locations on the plateau surface at an elevation of 900 m (Analavelona Plateau near Toliara; Figure 1b) in the southwest and at 300–500 m at the northernmost tip of the island (Roig et al., 2012; Stephenson et al., 2019), suggesting that the island has been

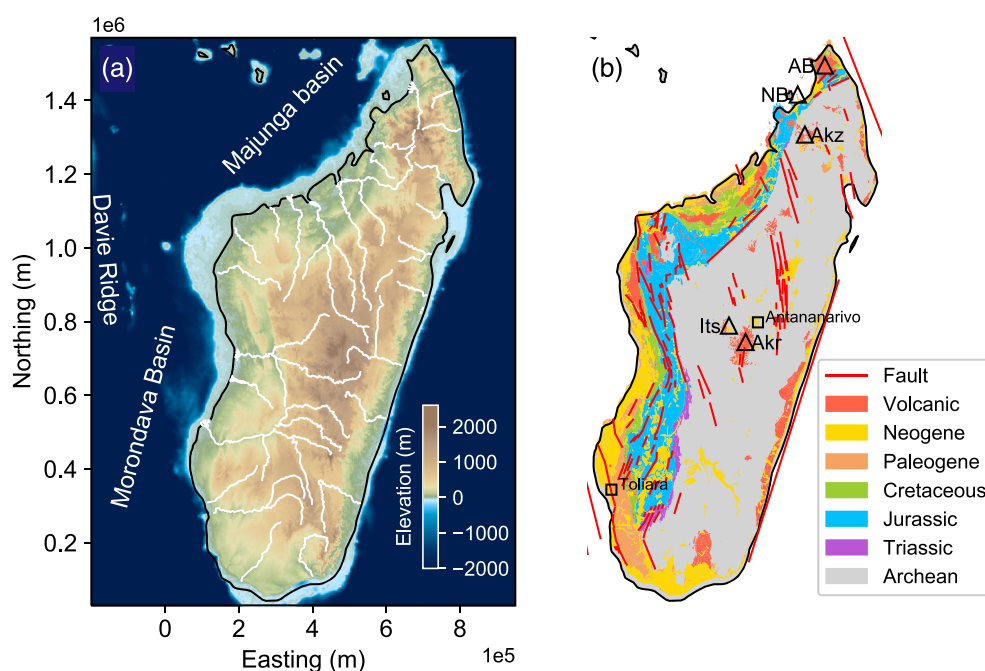


FIGURE 1 (a) Topography and bathymetry of Madagascar. White lines indicate the courses of major rivers. (b) Simplified geology of Madagascar (after Roig et al., 2012). Triangles indicate Quaternary volcanoes: AB, Ambre-Bobaomby; NB, Nosy-Be; Akz, Ankaizina; Its, Itasy; Akr, Ankaratra [Color figure can be viewed at wileyonlinelibrary.com]

uplifted significantly during the Cenozoic. On the central plateau, dating of the overlying sediments suggests a period of uplift of the central island between the late Eocene (prior to 34 Ma) and the Miocene–Pliocene boundary (5.5 Ma) (Bésairie, 1973). Based on the inversion of river profiles across the entire island, Roberts et al. (2012) inferred a 1–2 km high dome-shaped tectonic uplift during the past ~15 Ma. The centers of the inferred doming spatially overlap the late Cenozoic volcanic fields (Cucciniello et al., 2011; Emerick & Duncan, 1982; Nougier et al., 1986), suggesting that the high topography of central Madagascar may be dynamically supported by upwelling in the sub-lithospheric mantle (Roberts et al., 2012). Recent seismic tomographic studies (Celli et al., 2020; Pratt et al., 2017) have imaged a low-velocity zones at 50–150 km depths beneath the north, central, and southwestern regions of the island, supporting the hypothesis that asthenospheric upwelling is the source of the late Cenozoic volcanism and uplift of Madagascar. Earthquake focal mechanisms and campaign and continuous GPS data from the island indicate an ongoing, east–west extension of the crust (Bertil & Marc Regnault, 1998; Grimison & Chen, 1988; Rindraharisaona et al., 2013; Saria et al., 2014; Stamps et al., 2018, 2021), suggesting the island being on a diffuse, extensional plate boundary as the southern extension of the East African Rift (Horner-Johnson et al., 2007; Kusky et al., 2010; Stamps et al., 2021).

2.2 | Planation surfaces

We use planation surfaces as constraints on the history of uplift on the island. Planation surfaces are large areas of flat or gently tilted bedrock surfaces, which form as products of regional-scale erosional events (Guillocheau et al., 2018; King, 1953; Orme, 2013). In non-glacial settings, a planation surface may be created by the degradation of a drainage divide, the backwearing of an escarpment, or the wave-cutting of a marine platform. Although on the southeastern Tibetan Plateau, low-relief surfaces were also suggested to have formed *in situ* due to drainage area loss during dynamic drainage network reorganization (Yang et al., 2015), such a mechanism does not apply to planation surfaces widely preserved in continental interiors with no intense tectonic deformation—for example, in Australia, Central and Southern Africa, India, and both North and South America. In these regions, high-elevation, low-relief plateaus formed due to relatively slow and long-wavelength uplift, which may result from buckling of the lithosphere due to far-field forces (Cloetingh & Burov, 2011) or from upwelling currents in the sub-lithosphere mantle (Braun, 2010).

Planation surfaces found in Madagascar are comparable to those identified in Africa, which can be classified into two main types called pediplains (or pediments) and etchplains (Guillocheau et al., 2018). Their formation mechanisms differ in whether chemical weathering played a significant role or not. Pediplains (large in area) and pediments (smaller features) are mainly produced by physical erosion, most likely by large-scale sheet floods or highly avulsionary rivers (Dohrenwend & Parsons, 2009). Conversely, on top of an etchplain, strong chemical weathering associated with hot and humid climate leads to the formation of a thick lateritic mantle, which can be partially eroded later (Twidale, 2002). Overall, regardless of whether chemical weathering was involved, a planation surface is generally considered to originate at base level and only preserved following a period of

uplift or base level drop. In Madagascar, considering the relative small area of the island (compared to, e.g., the continent of Africa), it is reasonable to assume the sea level as the base level of erosion.

In Madagascar, the planation surfaces appear as flat or slightly warped small patches or large platforms (Figure 2), dissected by steeply incised river valleys. Assuming a relative stationary base level over the geological time scale, the current elevation of a surface records the total uplift accumulated since its formation—that is, the time when it was abandoned as the erosional base level. Moreover, vertical offsets between two surfaces record the incremental uplift magnitude over a period that is bounded by the ages of the two surfaces. Throughout the island, Delaunay (2018) mapped planation surfaces formed at nine different ages, based on interpreting their spatial relationship from field observations and a 90 m SRTM digital elevation model. In some places, these surfaces are covered by sedimentary layers or volcanic deposits, the ages of which can be used as constraints of the minimum ages of the underlying planation surfaces. Based on these age constraints and the regional geological history, Delaunay (2018) proposed an age model for the planation surfaces in Madagascar, as summarized below.

The oldest two surfaces (S_i and S_{ii}) are preserved only at very high altitudes in the center of the island, with ages older than the separation of the island from India (Bésairie, 1973; Dixey, 1960); these two planation surfaces are not used in our model. After Madagascar became an island, the oldest planation surface (S_{iii}) formed at ~90 Ma, and the next surface (S_{iiib}) formed after 84 Ma. Since the beginning of the Cenozoic, Madagascar has experienced a long history of tectonic quiescence, with neither uplift nor planation surfaces formation until the late Eocene. In the Cenozoic, the oldest planation surface (S_{iv}) formed between 38 and 31 Ma, concurrent with the uplift of the carbonate platforms around the island (Roig et al., 2012; Stephenson et al., 2019). Subsequently, two planation surfaces (S_{va} and S_{vb}) formed during the Miocene, 23–12 and 12–5 Ma, respectively. After the Miocene, the planation surface S_{vi} formed at or after 3.6 Ma. The youngest planation surface on the island formed since the Quaternary, associated with the most recent phase of the uplift of the island.

2.3 | Regional climate history

The relative intensity between chemical weathering and physical erosion is key to understanding the long-term evolution of planation surfaces and hence the evolution of the Malagasy topography. As shown by Gaillardet et al. (1995) for a modern system over a very short period, under humid climate (i.e., Congo River over one year), close to 40% of the eroded volumes are due to chemical weathering. According to the data compiled from the 60 largest rivers in the world (Gaillardet et al., 1999), the rock weathering rate is strongly dependent on the climate conditions (i.e., precipitation and temperature). Other factors affecting the weathering rate include lithology and physical erosion rate.

The climate history of Madagascar is still under debate and past studies have been based on pollen analysis (e.g., Buerki et al., 2013; Wells, 2003) or numerical models (Ohba et al., 2016). During the Late Cretaceous Madagascar was located between 30 and 40° S (van Hinsbergen et al., 2015) in a zone of arid climate (Blakey, 2008; Wells, 2003). During the latest Cretaceous (85–65 Ma), a transition to

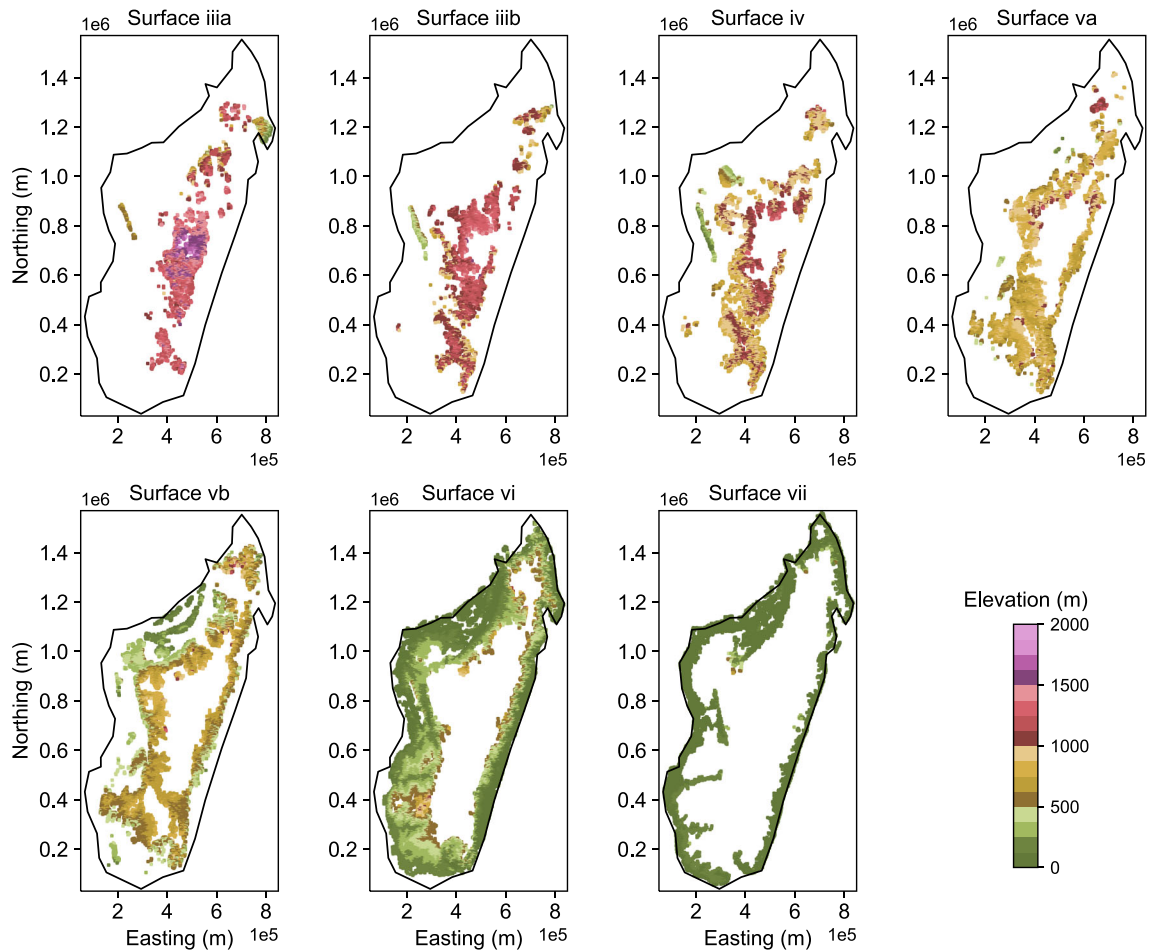


FIGURE 2 Remnants of pediment surfaces in Madagascar mapped by Delaunay (2018). Only surfaces formed after 90 Ma are shown. Formation ages of surfaces were estimated at (iiiia) 90–84 Ma, (iiib) 84–66 Ma, (iv) 41–29 Ma, (va) ~11 Ma, (vb) ~5 Ma, (vi) <3.6 Ma, and (vii) the Quaternary, and prescribed in the our model at 90, 84, 34, 11, 5, 3, and 2.6 Ma, respectively [Color figure can be viewed at [wileyonlinelibrary.com](https://onlinelibrary.wiley.com)]

a very humid environment was recorded by changing vegetation types (*Takhtajania perrieri* and *Dilobeia* Buerki et al., 2013; Marquinez et al., 2009), and was recently confirmed in wells offshore Mozambique (Ponte et al., 2019). Warm and humid conditions continued to prevail through the Paleocene and Eocene, as the island moved northwards. According to the fossil records from southern Africa, the climate changed to a more arid setting (Braun et al., 2014; Ponte et al., 2019) at the beginning of the Oligocene, and back to very humid conditions at the mid-Oligocene and humid conditions at the Oligo–Miocene boundary. Since the Miocene, the island has presented a climate partitioning between the relatively arid side to the west and humid to the east. During the middle Miocene (since ~16 Ma), the island overall was in a semi-arid condition, but since the late Miocene (~11 Ma) alternation between dryer and wetter conditions started and continue to the present.

2.4 | Sediment volume data

We use the volume data of the siliciclastic sediment from the Morondava Basin (Delaunay, 2018) as a main constraint for the landscape evolution models. The Morondava Basin is located southwest of Madagascar (Figure 1a). Along its western margin, this deep marine basin is bounded by a prominent bathymetric high—the Davie Ridge—

which is commonly regarded as a transform boundary formed during the break-up between Africa and Madagascar (e.g., Mahanjane, 2014); the latter was still part of Antarctica at that time. As a consequence, the basin has stored most of the terrigenous sediment that was shed off the southwest coast of Madagascar, first during the continental rifting from late Carboniferous to Early Jurassic (Geiger et al., 2004; Piqué et al., 1999; Wescott & Diggins, 1997, 1998), and then in a passive margin setting since the Middle Jurassic (Geiger et al., 2004; Geiger & Schweigert, 2006).

Delaunay (2018) estimated the incremental thickness and volume of sediment in the offshore and onshore parts of the Morondava Basin, between the Archean and Proterozoic basement to the present-day seafloor/surface. We use his estimates for the time period between ~90 Ma and the present as model constraints, as older sediment deposits were disrupted by the rifting process and only partially preserved. According to Delaunay (2018), the total volume of terrigenous siliciclastic sediments between ~90 and 0 Ma is estimated at $(131.7 \pm 29.4) \times 10^3 \text{ km}^3$ (Table 1). Sediments accumulated predominantly during two periods: one in the Late Cretaceous (~90–66 Ma) and the other in the late Cenozoic (~34–0 Ma). From ~90 to 66 Ma, the average volumetric sedimentation rate was $(1.3 \pm 0.2) \times 10^3 \text{ km}^3/\text{Ma}$, and the sediments were mainly siliciclastic. During the Paleocene and Eocene (~66–34 Ma), clastic sedimentation was negligible. Late Cenozoic sedimentation started in the Oligocene,

TABLE 1 Sediment volume in the Morondava Basin since ~90 Ma (Delaunay, 2018)

Time interval (Ma)	Volume ($\times 10^{12} \text{ m}^3$)	σ ($\times 10^{12} \text{ m}^3$)
90–66	30.2	5.9
66–34	2.3	2.3
34–23	16.7	3.7
23–12	20.2	4.0
12–5	38.3	8.3
5–0	24.1	5.2

with a gentle increase in sedimentation rate during the early Miocene. A marked acceleration of the sedimentation occurred during the mid-Miocene, when the volumetric sedimentation rate jumped from $(1.8 \pm 0.4) \times 10^3$ to $(5.5 \pm 1.2) \times 10^3 \text{ km}^3/\text{Ma}$. Since the Pliocene, the sedimentation rate has decreased slightly, to $(4.8 \pm 1.0) \times 10^3 \text{ km}^3/\text{Ma}$.

3 | LANDSCAPE EVOLUTION MODELING

3.1 | Forward model

To simulate landscape evolution, we assume that the erosion of Madagascar was dominated by fluvial erosion and hillslope processes. Instantaneous elevation change is computed by using an adjusted version (Davy & Lague, 2009) of the stream power law (e.g., Howard, 1994; Whipple & Tucker, 1999) and a linear hillslope diffusion (Culling, 1960):

$$\frac{\partial h}{\partial t} = U - \max(0, K_f A^m (\nabla h)^n - \dot{\epsilon}_c) + K_d \nabla^2 h, \quad (1)$$

where U is the uplift rate, h is the elevation, t is time, A is the upstream drainage area, ∇h is the local relief; K_f is the erosion coefficient, whose value is dependent on factors such as rock erodibility, and varies over a few orders of magnitude; we will optimize its value through the inverse modeling process (Section 4). Exponents in the erosion law (m and n) dictate the degrees of dependence of the predicted erosion rates on topographic parameters such as upstream drainage area and local channel slope. The value of K_d is strongly dependent on the spatial resolution of the model, and the ratio between K_f and K_d also determines the relative efficiency between long- and short-distance processes as well as the resultant density of river networks. For the efficiency of our inverse modeling, we fix the values of m , n , and K_d at 0.4, 1, and 0.1, respectively. These are within the ranges of commonly estimated or assumed values (m/n , 0.35–0.6; n , 0–4; K_d , 0.01–10). A recent study in southern Africa (Stanley et al., 2021) followed similar assumptions, and our adopted values were among those used to simulate the landscape evolution of passive margins (Braun, 2018). In addition, our initial experiments show that different values of m and n will affect the estimated values of K_f , but have insignificant impacts on the sediment volumes predicted by the optimized models. In addition to the classical stream power law, we follow Davy and Lague (2009) and add a threshold erosion rate, $\dot{\epsilon}_c$, such that fluvial erosion is only effective where the shear

stress is above a threshold. The value of $\dot{\epsilon}_c$ is also constrained by inversion. We use the FastScape algorithm (Braun & Willett, 2013) and the alternating direction implicit method (Peaceman & Rachford, 1955) to solve the stream power erosion and the hillslope diffusion equations, respectively. Both methods are implicit and therefore stable for modeling landscape evolution using relatively large time steps.

3.2 | Uplift model

We prescribe the uplift functions based on the vertical offsets between the planation surfaces mapped by Delaunay (2018), through the following steps: (1) we divide the model space into a 16×32 grid, and calculate the median elevation of the planation surfaces within each cell (of area $50 \times 50 \text{ km}^2$); (2) using the median elevations, we calculate the offset between each planation surface and the subsequent surface (Figure 3), and use it as the proxy for the accumulated uplift during the period between the times when the two surfaces formed; (3) we interpolate and extrapolate the estimated uplift functions to the 400×800 model grid (of area $2 \times 2 \text{ km}^2$); (4) finally, we smooth the uplift functions and filter out uplift signals with $<500 \text{ km}$ wavelength (Figure 4). Based on ranges of formation ages of the planation surfaces constrained in Delaunay (2018), we arbitrarily assign ages of the seven planation surfaces—that is, iiaa, iiib, iv, va, vb, vi, and vii, at 90, 84, 34, 11, 5, 3, and 2.6 Ma, respectively; the Mesozoic uplift is set to stop at 66 Ma, corresponding to the onset age of minimal sedimentation in the Morondava Basin (Piqué et al., 1999). We acknowledge the existing uncertainties in the age constraints of the planation surfaces. However, given the long time intervals (5 to $>30 \text{ Ma}$) over which the sediment volumes were estimated, we argue that the inverse modeling directed by these estimates is not sensitive to the variations in ages of the planation surfaces within the inferred constraints.

Our model of the landscape evolution of Madagascar starts in the Late Cretaceous at 90 Ma, when the planation surface iiaa was abandoned as the erosion base level. This surface formed after the break-up between Madagascar and India, and therefore recorded the oldest uplift history of the island since its separation from other continents. At this time, the continent of western Madagascar along the Majunga and Morondava Basins was submerged. The remainder of the island areas presented as extensive, low-elevation plains directly connected to the ocean. An uncertainty exists for the topography of the eastern margin of the island, where, following the Madagascar–India rifting, remnants of the continental shoulders could remain or have been degraded. Therefore, we use two parameters to prescribe the initial topography of the model: H_0 is the elevation along the western margin of the island and H_1 is that along the eastern margin, and a linear, eastward increase is imposed for elevations between the two margins. Both H_0 and H_1 will be optimized in the inversion (Section 4). The initial topography is imposed on a 400×800 grid and covers the area of the continental lithosphere of Madagascar.

Each step of the landscape evolution model is 100 ka long and correspondingly a total of 900 steps is simulated. We divide the model time into seven episodes of uplift (Figure 4), and each episode is bounded by ages of two subsequent planation surfaces; the only exception is the second episode, which starts at 84 Ma

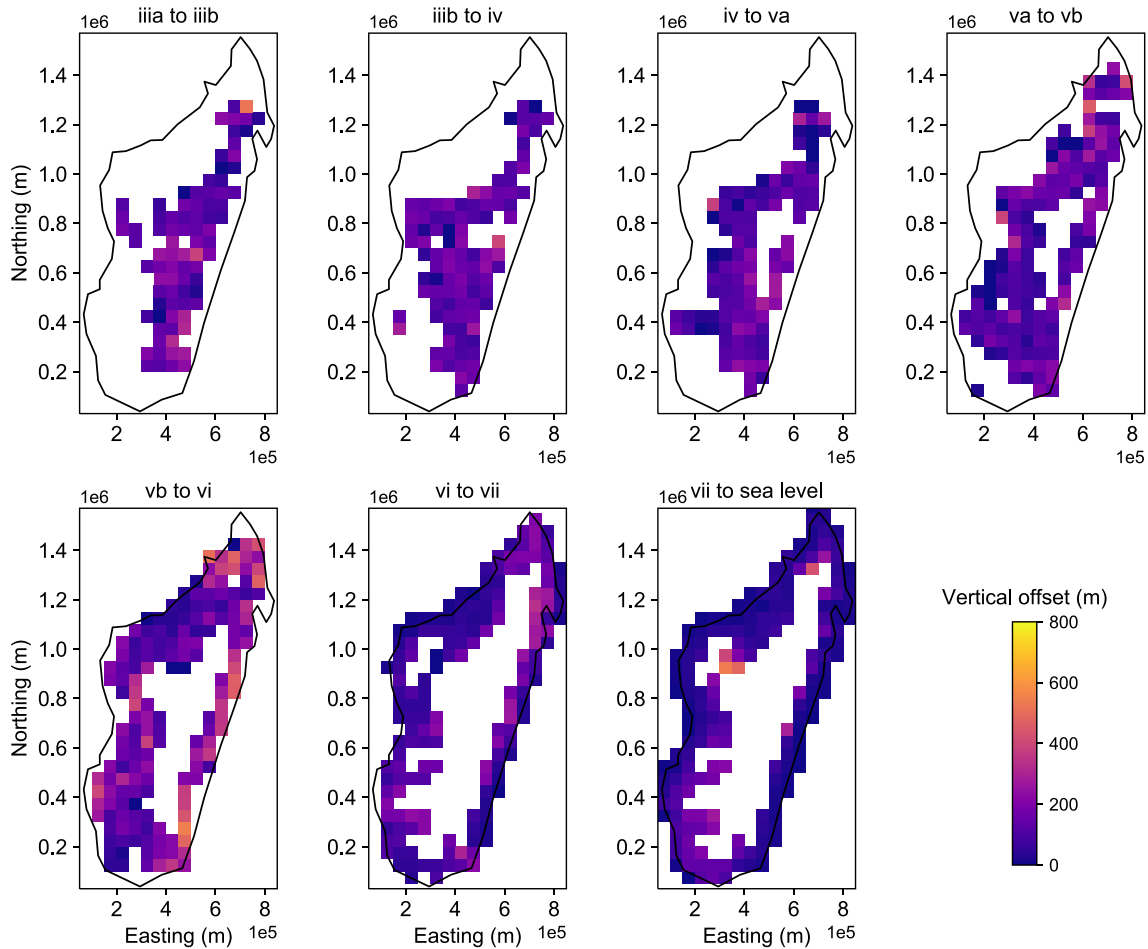


FIGURE 3 Vertical offsets between two planation surfaces. The offsets are calculated on a 16×32 grid of $50 \times 50 \text{ km}^2$ cells using the median elevation of the surfaces within each cell [Color figure can be viewed at wileyonlinelibrary.com]

(age of the surface iiib) but terminates at the end of Cretaceous (66 Ma). During each episode, the uplift rate of a given location is set to remain constant—that is, the vertical offset between planation surfaces divided by their age difference.

3.3 | Inverse modeling

We use the Neighbourhood Algorithm (Sambridge, 1999) to optimize the parameters in the erosion laws (K_f and $\dot{\epsilon}_c$ in Equation (1)), the elevations on the western and eastern margins of the initial topography, and the ratios of sediment loss (see below in this section). The inversion method is proven to be an efficient scheme for constraining the values of unknown parameters in a multi-dimensional space (Sambridge, 1999). During each iteration, the parameter space is uniformly divided into Voronoi cells defined by combinations of parameter values, and models in centers of the cells are assessed using defined misfit functions. The subsequent iteration repeats the process but within a reduced parameter space that is defined by models with lowest misfits from previous iteration. Optimization of the forward model is achieved by performing a large number of iterations. The sampling ranges and results for parameters in our inversion are listed in Table 2.

The inversion is constrained by the present-day topography and sediment volume data from the Morondava Basin. As the evolution of

a natural landscape is a stochastic process, it is unrealistic to reproduce the exact natural topography with the LEM. We choose to minimize the difference between the cumulative density functions (CDFs) of the elevations between the present-day Madagascar and the final topography predicted by the LEM.

As a portion of the eroded materials may be consumed by chemical weathering, to fit the sediment volume data we impose a sediment loss ratio to represent the portion of the erosion products that were not preserved in the offshore basin. Assuming a strong dependence of chemical weathering intensity on climate (Gaillardet et al., 1999), we assign an independent sediment loss ratio for each of the seven climate periods (Section 4)—that is, c_1 to c_7 for 90–85, 85–34, 34–29, 29–23, 23–16, 16–11, and 11–0 Ma, respectively. In the inverse modeling, all ratios are searched in the range of 0–0.5. Our approach ignores recycling of sediment, and therefore sometimes could potentially underestimate eroded volume. However, the recycling of sediments should be restricted to the relatively small areas in the lowlands along the west coast, and we therefore consider sediment recycling as a secondary process.

During the inversion, we compute the misfits in elevation and sediment volume data separately, and then combine them using the equation

$$\phi = aD + b \sum_{i=1}^N \log \left(\frac{V_{o_i} - V_{p_i}}{\delta_i} \right)^2, \quad (2)$$

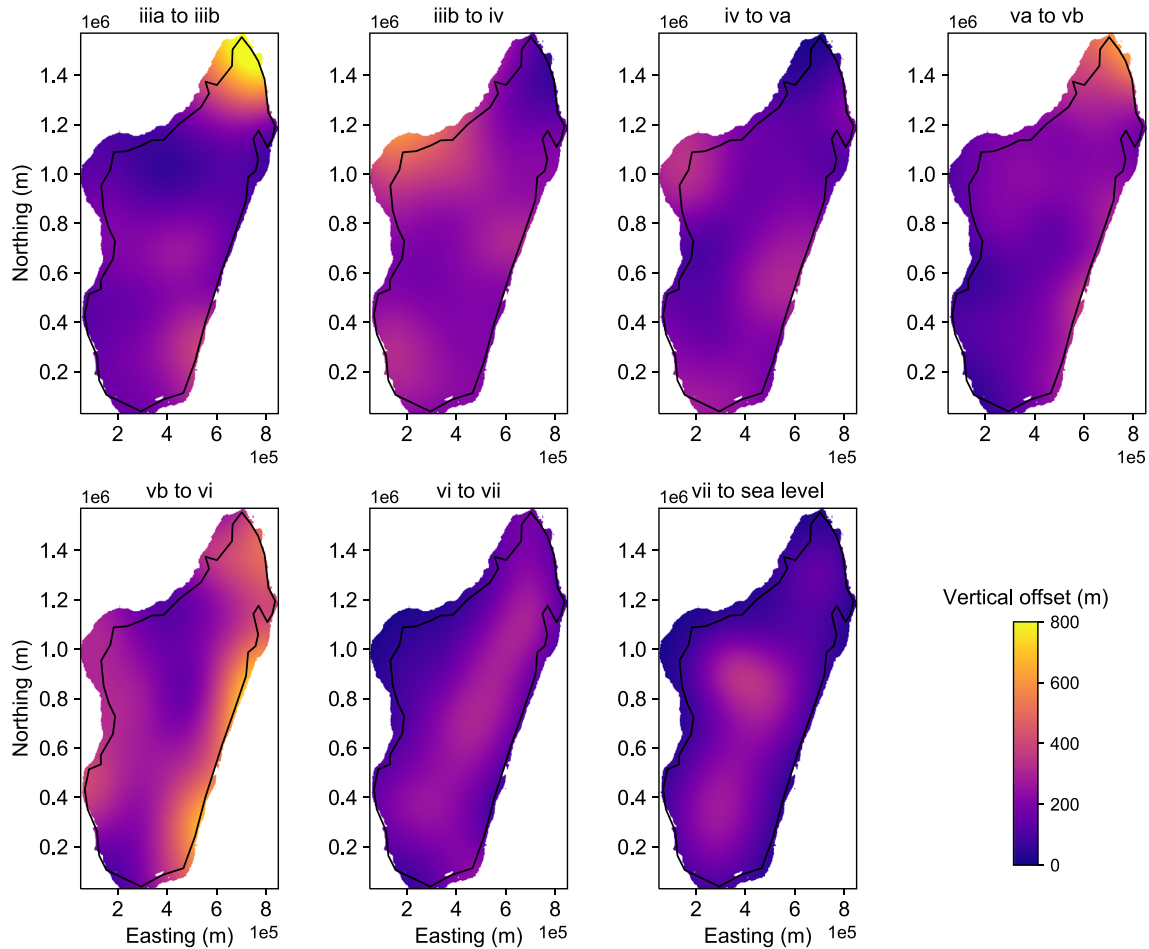


FIGURE 4 Interpolated and extrapolated uplift magnitudes between two planation surfaces. The uplifts are calculated on a 400×800 grid of $2 \times 2 \text{ km}^2$ cells and used in the landscape evolution model as uplift magnitudes accumulated for the episodes of 90–84, 84–66, 34–11, 11–5, 5–3, 3–2.6, and 2.6–0 Ma, respectively [Color figure can be viewed at wileyonlinelibrary.com]

TABLE 2 Model parameters sampled in inversion

Parameter	Code	Range	Unit	Best fit
Logarithm of erosion coefficient	$\log(K_f)$	–6 to –3	$\log(\text{m}^{0.2}/\text{yr})$	–5.195
Logarithm of erosion rate threshold	$\log(\hat{e}_c)$	–6 to –1	$\log(\text{m}/\text{yr})$	–4.819
Initial elevation in the west	H_0	–200 to 0	m	–32
Initial elevation in the east	H_1	0–1000	m	28
Sediment loss ratio (90–85 Ma)	c_1	0–0.5		0.34
Sediment loss ratio (85–34 Ma)	c_2	0–0.5		0.49
Sediment loss ratio (34–29 Ma)	c_3	0–0.5		0.19
Sediment loss ratio (29–23 Ma)	c_4	0–0.5		0.02
Sediment loss ratio (23–16 Ma)	c_5	0–0.5		0.04
Sediment loss ratio (16–11 Ma)	c_6	0–0.5		0.15
Sediment loss ratio (11–0 Ma)	c_7	0–0.5		0.50

where D is the Kolmogorov–Smirnov (K-S) statistic between the CDFs of natural and predicted elevations, v_o and v_p , and observed and predicted sediment volumes, respectively, and N is the number of sediment volume data points (or time intervals). Two scaling coefficients, a and b , are used to calculate a combined misfit. We tested the values of a and b by trial and error, attempting to keep the two components of misfit at the same order of

magnitude; both parameters were finally prescribed at 1. The inversion presented here comprises a sum of 200 iterations. The first iteration includes 1000 forward runs, and each of the following 250 iterations. We use a resampling ratio of 0.8—that is, a random walk in 200 out of the 250 cells from the previous run—to reach a balance between convergence rate and a reasonable exploration of the parameter space.

4 | RESULTS

The inversion processes showed good convergence for all sampled parameters except H_0 . The performance of the modeling is presented here as frequencies of the sampled sediment loss ratios (c_1 – c_7) in the seven climate periods (Figure 5) and projections of a thinned (20%) assemblage of sampled erosion law parameters onto 2D planes (Figure 6). We also show the estimated density functions for the exhumation rates at three locations in the north, center, and south of the island, in comparison with their uplift functions prescribed at the respective sites (Figure 7).

The modeling results suggest that throughout the island the predicted erosion rates are mostly consistent with the rock uplift rates, until at least the late Miocene (<10 Ma) (Figure 7). During the Late Cretaceous, the island experienced slow erosion with rates most likely <0.07 km/Ma; large uncertainties for the initial period (90–

85 Ma) of the model exist, likely due to the uncertainty in the initial topography of the model (Figure 7). The Late Cretaceous uplift and erosion ceased prior to ~50 Ma. The Cenozoic erosion started in response to the rejuvenated uplift of the island near the Eocene–Oligocene boundary, but the rates had remained low (Figure 7). For all parts of the island, uplift rates increased in the late Miocene (~12 Ma). However, associated with this event the models predict no significant increase in the erosion rates, except in the north, where the models suggest a delayed feedback of erosion rate increase. A more marked acceleration in uplift rates occurred at 5 Ma, when the rates at the selected sites increased from <0.05 to >0.2 km/Ma (Figure 7). In response to this event, substantial increases in erosion rates are predicted throughout the island. By the end of the model time (with the exception of the north of the island), erosion rates had not adapted to the same magnitudes as the most rapid uplift rates prescribed for the Pliocene period (Figure 7).

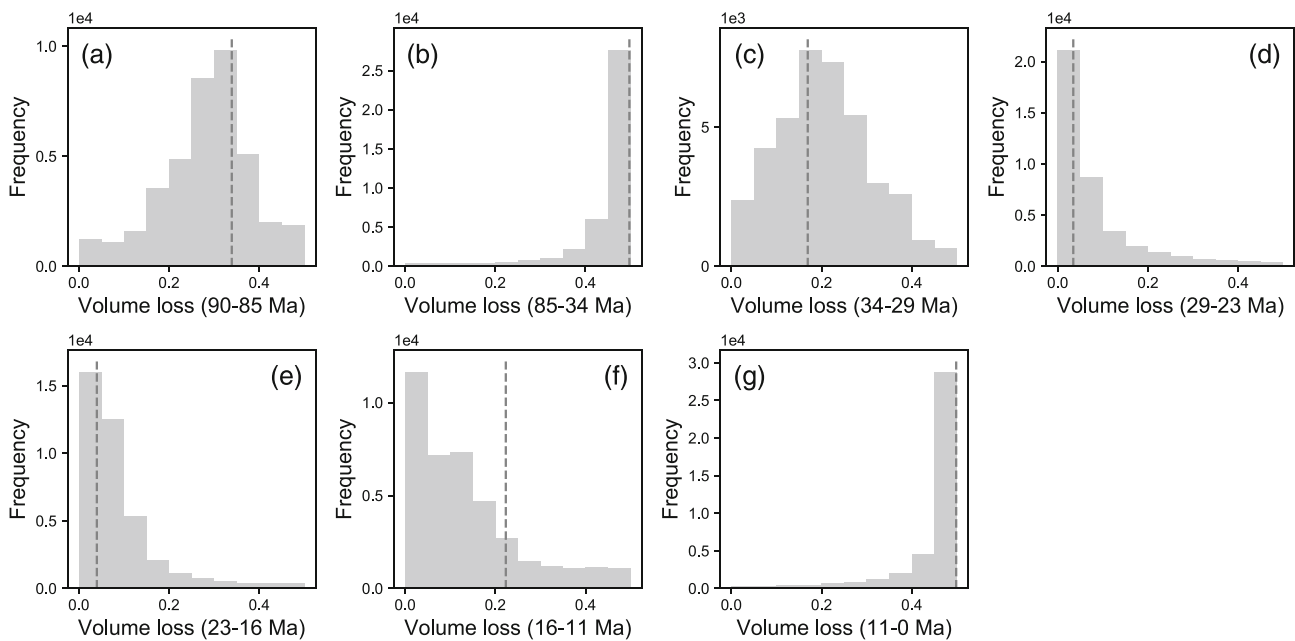


FIGURE 5 Inverse modeling results of the sediment volume loss. Distributions of sampled values are shown for prescribed climate periods of (a) 90–85 Ma, (b) 85–34 Ma, (c) 34–29 Ma, (d) 29–23 Ma, (e) 23–16 Ma, (f) 16–11 Ma, and (g) 11–0 Ma, respectively. Dashed vertical lines indicate the values of the best-fit model

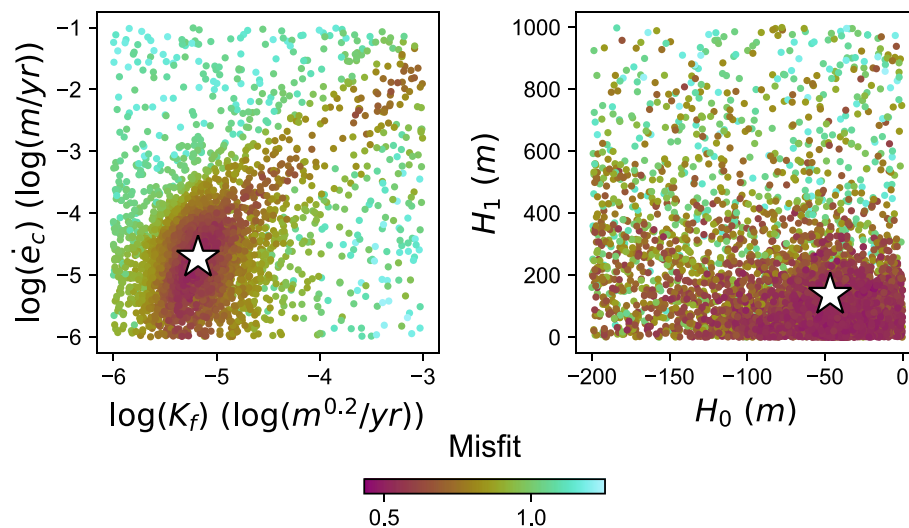


FIGURE 6 Inverse modeling results of K_f , \dot{e}_c , H_0 , and H_1 . Results are shown as a thinned (20%) ensemble of sampled forward models projected onto planes defined by pairs of parameters. Color indicates the misfit of a forward model, and a star depicts the “best-fit” model [Color figure can be viewed at wileyonlinelibrary.com]

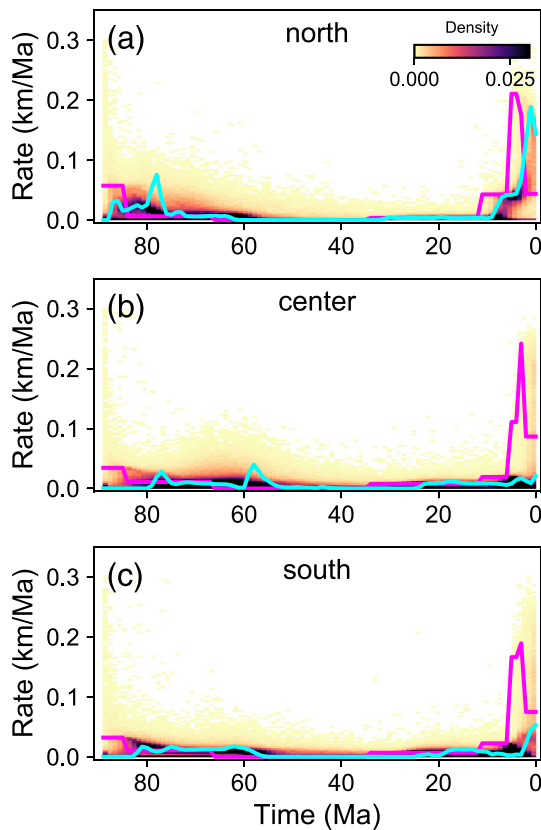


FIGURE 7 Rock uplift and predicted erosion rates at three representative sites in the (a) north, (b) center, and (c) south of Madagascar. Site locations are shown in Figure 8. Magenta lines depict the uplift model. Modeled erosion rates are shown as probability density functions calculated from a thinned assemblage (20%) of the sampled forward models; cyan lines depict erosion rates of the best-fit model [Color figure can be viewed at wileyonlinelibrary.com]

Figure 8 shows the topographic history predicted by a best-fit model. The initial topography of the model is made of a low-relief surface gently tilted to the west. During the Late Cretaceous, the model predicts an increase in onshore area associated with the uplift of the island. Since the Cenozoic, the onshore area has had a similar shape to the present-day island, but the elevation remained low (<500 m) prior to 10 Ma. During the last ~10 Ma, the modeled elevation of the island increased significantly. However, the best-fit model cannot reproduce some details from the landscape of the modern Madagascar—for example, distribution of the low-relief central plateau and the asymmetry in the drainage areas between basins draining to the west and those to the east (Figure 1a)—which indicates the potential limitation of the current model (Section 4).

5 | DISCUSSION

5.1 | Limitations of the modeling

It is possible that during the early Cenozoic Madagascar experienced a period of subsidence, as evidenced by the carbonate platform preserved along the west coast. This event could decrease the land area and hence reduce the sediment flux into the Morondava Basin. As the planation surfaces could not record the magnitude of the surface

downwarping, we did not implement any subsidence (i.e., negative uplift) in the modeling. Instead, we prescribed a period of zero uplift rate, which effectively resulted in a time span with minimum erosion and sediment flux (Figures 9a and 11a). As the net uplift for a time period is decided by the offset between planation surfaces, ignoring the subsidence could lead to potential underestimates of the uplift magnitude and rate over the period immediately following the subsidence—that is, 34–12 Ma. However, with the current setup our model agrees well with the uplift history of the island inferred from river profile inversion (Roberts et al., 2012; Stephenson et al., 2021), in which the average uplift rates were low (~0.01 km/Ma) before 20 Ma and rapid uplift did not start until the mid- to late Miocene. Therefore, we suggest that ignoring the early Cenozoic subsidence is a reasonable simplification of the uplift model.

The modeling results do not fully replicate the modern topography of Madagascar (Figure 9b). In particular, the numerical model cannot reproduce the bimodal distribution of the elevation data, which represents an extensive, elevated low-relief plateau in the center of the island and extensive plains connected to the coast (Figure 1a). We suspect that this discrepancy is at least in part due to the limitation of the forward erosion model: a combination of the fluvial incision and hillslope diffusion cannot fully reproduce the high-elevation, low-relief surface. Adding a threshold on the stream power could help preserve some of the relict surfaces (e.g., Stanley et al., 2021). However, as the physical process of planation (e.g., sheet floods) is not simulated by the LEM, the models cannot generate an expansive pediplain or etchplain at the base level, and thus the low-relief surfaces also do not occur extensively on the high plateau on the final landscape (Figure 8). This imperfection may be improved by incorporating into the forward model additional components that simulate more surface processes, such as chemical weathering (Braun et al., 2016) or sediment deposition (Yuan et al., 2019). However, in order to focus on the relationship between uplift and sedimentation and reduce the dimension of the inverse problem, we opted for a simple LEM rather than a complete recovery of the natural landscape.

Our misfit function based on the K-S statistics of the DEM (Equation 2) is constructed with the aim to reproduce the general range of the elevations of the island, and thus is insensitive to the pixel-wise shape of the topography. Therefore, specific features of the landscape, such as drainage basin geometry and location of the escarpment on the east coast, are not monitored during the inversion. As our uplift function is prescribed and initial topography is very simple, such detailed features of the topography are almost impossible to reproduce without imposing spatial variability in the rock erodibility or the precipitation intensity.

5.2 | Uplift and erosion model

The fluvial incision coefficient was sampled in the logarithmic space, and $\log(K_f)$ converged to the range of -5.5 to -5 (Figure 6a), which is within the range of values commonly adopted by landscape evolution studies (e.g., Whipple & Tucker, 1999). The logarithm of the erosion threshold, $\log(\hat{e}_c)$, is constrained to the range of -5 to -4.5 (Figure 6a). The optimized values of the two parameters show an apparent positive correlation. This can be expected, as we impose the sediment yield and therefore the mean erosion rate of the landscape;

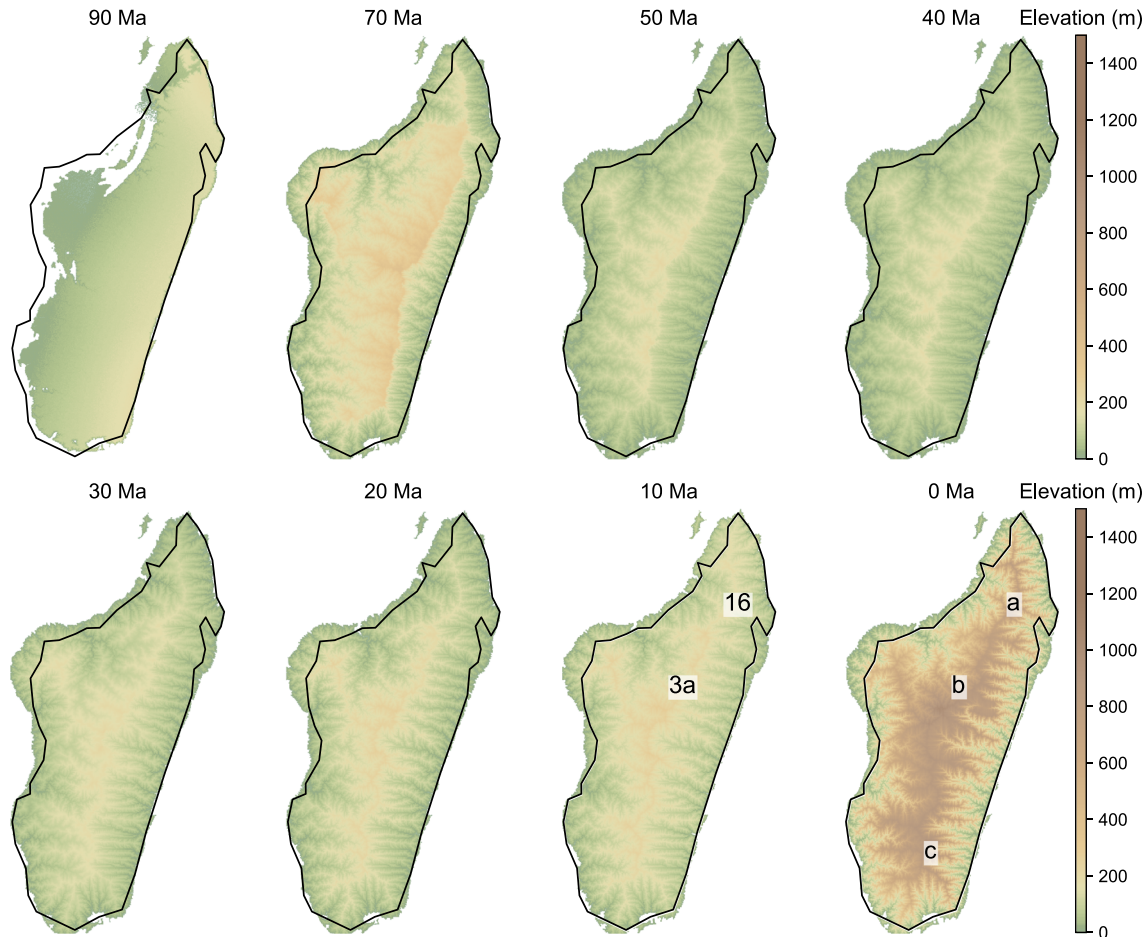


FIGURE 8 Evolution of the topography predicted by the best-fit model. Sites a, b, and c indicate locations where uplift and erosion histories are calculated (Figure 7). Sites 3a and 16 are locations where rock cooling models are calculated (Figure 10) [Color figure can be viewed at wileyonlinelibrary.com]

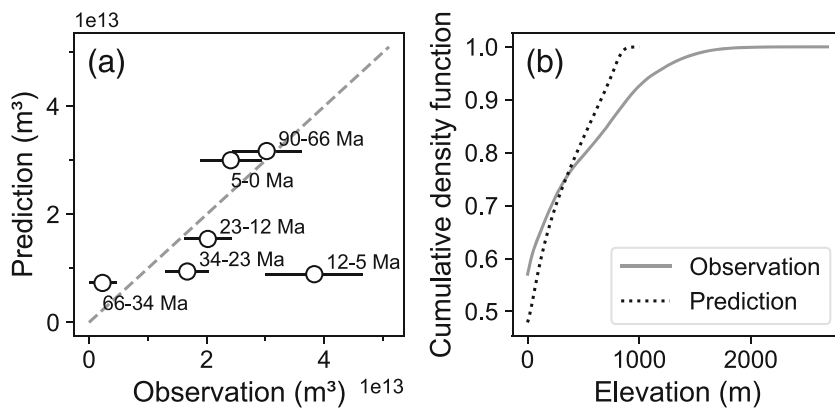


FIGURE 9 Predictions of the best-fit model compared to observations. (a) Observed versus predicted sediment volumes in the Morondava Basin. (b) Cumulative density functions (CDFs) of the present-day topography (observation) and the DEM at the final stage of the landscape evolution model (prediction)

thus, a higher threshold for the minimal erosion rate in the headwaters or low-relief regions requires to be balanced by higher efficiency in the fluvial incision rate in lower reaches or steep sections of rivers. The same correlation between the fluvial incision efficiency and erosion threshold was also observed in the inverse modeling presented in Stanley et al. (2021), which was used to inspect the uplift and erosion history of southern Africa. Moreover, the optimized value of K_f is most consistent with the results ($\log(K_f) \approx -5.5$) of the “hybrid early scenario” model of Stanley et al. (2021), which in addition to the Cretaceous uplift involves a phase of early Cenozoic uplift due to the mantle process; the similar, two phases of uplift history are also used

in our models. Therefore, if the same erodibility can be assumed for the bedrocks from southern Africa and Madagascar (both predominantly Precambrian basement), our results support a consistency in the uplift and erosion scenarios between models of southern Africa and Madagascar. This general synchronization implies that the geodynamic processes responsible for the Cenozoic uplift of the two regions were connected, perhaps both subject to the development of the East African Rift system (Cucciniello et al., 2018; Ebinger & Sleep, 1998).

By inverting the geometry of long river profiles, Roberts et al. (2012) and Stephenson et al. (2021) estimated the fluvial erosion

coefficient K at $2 \times 10^{-4} \text{ m}^{0.6}/\text{yr}$ and $4 \times 10^{-6} \text{ m}^{0.3}/\text{yr}$, respectively. Based on their modeling results, both Roberts et al. (2012) and Stephenson et al. (2021) suggest a period of Cenozoic uplift to construct the high plateau of Madagascar. Based on basin averaged erosion rates estimated from cosmogenic ^{10}Be concentration, Wang et al. (2021) calibrated the erosion coefficient K at $2 \times 10^{-6} \text{ m}^{0.3}/\text{yr}$ ($m/n=0.35$) or $4 \times 10^{-7} \text{ m}^{0.1}/\text{yr}$ ($m/n=0.45$). The low erosion rate inferred from ^{10}Be is consistent with a model of continuous retreat of the great escarpment on the east coast since the Cretaceous rifting of the India–Madagascar margin, without the necessity for a renewed phase of uplift during the Cenozoic. The estimated K value of our best-fit model is about $6 \times 10^{-6} \text{ m}^{0.2}/\text{yr}$, lower than the calibration of Roberts et al. (2012) but higher than Stephenson et al. (2021) and Wang et al. (2021). Considering that our erosion model includes a threshold for minimum erosion, it is reasonable for our estimates to be slightly higher; we also demonstrate that the estimate of K value tends to reduce with a decreasing erosion threshold $\dot{\epsilon}_c$. The uplift function in our model is extracted from the distribution of planation surfaces of Delaunay (2018), which also invoke a Cenozoic period of uplift, consistent with inferences of Roberts et al. (2012) and Stephenson et al. (2021). However, an observation emerges from our 2D planview model: if spatial variability in the uplift rates existed, dynamic reorganization of the river networks would have been active near the main drainage divide, including captures of stream channels between the west- and east-draining rivers. Therefore, as pointed out by Wang et al. (2021), assumptions of stationary upstream drainage areas, upon which the inversion of river long profiles is based, could be problematic. On the other hand, as the misfit function in our inverse modeling is insensitive to the geometry of the drainage basin, our results are not suitable for negotiating between the models of Cenozoic uplift and low erosion rates on the east coast.

Nevertheless, our models suggest that along the west coast and on the central plateau of Madagascar, the total magnitudes of exhumation since the India–Madagascar rifting have been low, and mostly occurred after the Miocene. By assuming a near-surface geothermal gradient of $\sim 25^\circ\text{C}/\text{km}$, we used a 1D heat diffusion model to calculate the cooling paths of rocks in the north and center of the island. The results show that these rocks were at temperatures $<50^\circ\text{C}$ since the Late Cretaceous (Figure 10). These predictions are consistent with the thermal history models derived from apatite fission-track and (U-

Th-Sm)/He data (Stephenson et al., 2021), confirming that the post-rifting magnitudes of exhumation on the central plateau of Madagascar could not “reset” the apatite low-temperature thermochronology systems (Emmel et al., 2012; Seward et al., 2004; Stephenson et al., 2021).

5.3 | Volume balance between erosion and sedimentation

The results of our inverse modeling of the landscape evolution allow a semi-quantitative assessment of the sediment balance between the source and sink. In southern Africa, Rouby et al. (2009) documented a good volume balance between the terrigenous sediments in the basins along the west coast and the onshore erosion estimated from low-temperature thermochronology for the past 150 Ma, suggesting that over geological time scales the volume data can effectively reflect the evolution of the sediment provenance. Using the same proxies along the south coast of South Africa, Tinker et al. (2008) found much lower volumes of offshore sedimentation than onshore denudation, suggesting a substantial portion of the erosion products being removed from the system. Stanley et al. (2021) constrained landscape evolution models of the southern African plateau using topographic, sediment flux, and low-temperature thermochronological data, and found that the erosion volumes predicted by the best-fit models are significantly lower than the observation. After careful consideration of the possible factors, they attributed most of the sediment loss to chemical weathering, though some materials might also be transported out of the system by tectonic (transform faulting and rifting), oceanic (deep and surface currents), or eolian processes.

Our best-fit models suggest that most of the sediment loss occurred from the Late Cretaceous to Eocene and since the Pliocene; during the two periods, inversions of the sediment loss ratios both converge to the upper boundaries of the sampling spaces (Figure 5). The high sediment loss ratio during the Late Cretaceous is consistent with the best-fit models of Stanley et al. (2021), which predict that only one third of the erosion products accumulated in the basin. The high weathering intensity is supported by the very humid climate conditions from the Late Cretaceous to Eocene, recorded both globally

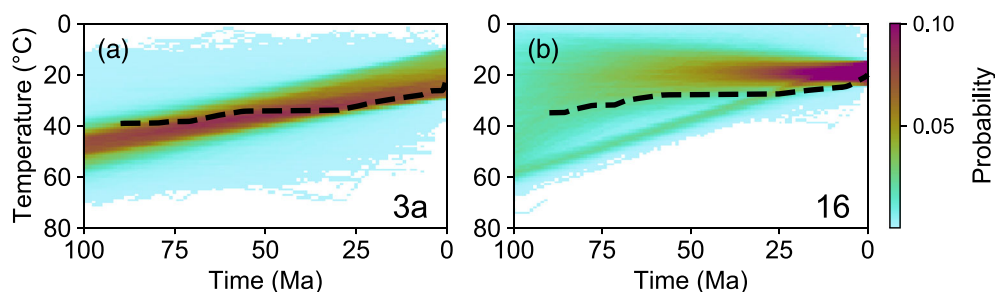


FIGURE 10 Rock cooling histories predicted by the best-fit landscape evolution model (dashed line) compared to results from inversion of thermochronological data (heat map). Dashed lines depict the prediction of the landscape evolution model, assuming a surface temperature at 20°C and a near-surface geothermal gradient at $25^\circ\text{C}/\text{km}$. Thermal history models reported by Stephenson et al. (2021) are reproduced, using the same data, approach, and setup. The modeling method is Bayesian transdimensional Markov chain Monte Carlo (Gallagher, 2012) and results are shown as the probability density function of the 400,000 post-burn-in models following the initial 100,000 burn-in. (a) and (b) present results using apatite fission-track and (U-Th-Sm)/He data of two samples 3a (a) and 16 (b) in Stephenson et al. (2021). Locations of samples are shown in Figure 8 [Color figure can be viewed at [wileyonlinelibrary.com](https://onlinelibrary.wiley.com)]

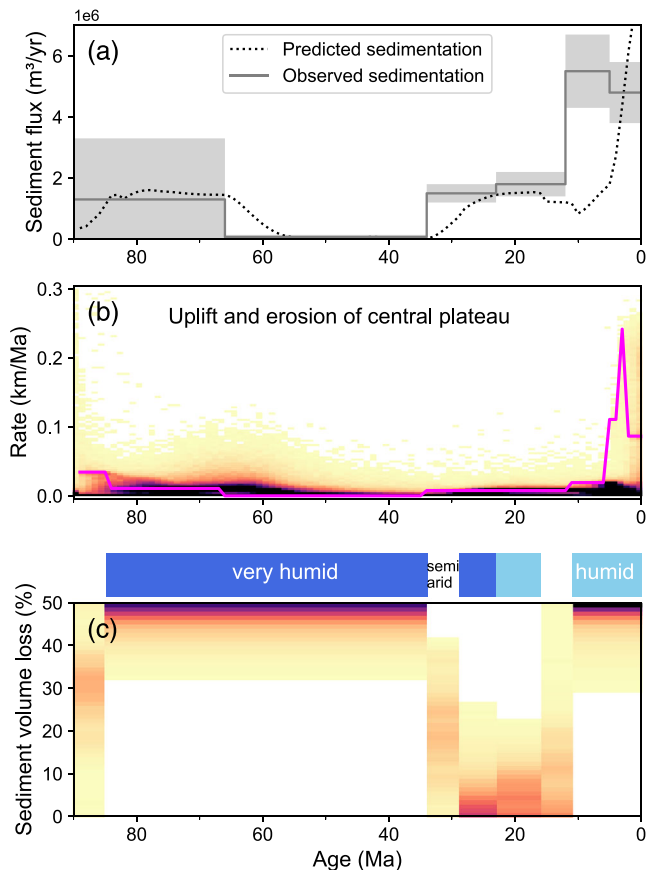


FIGURE 11 Summary of the uplift, predicted erosion and sedimentation histories in Madagascar. (a) Observed versus predicted sediment fluxes into the Morondava Basin. Grey shading indicates the uncertainty (σ) of the estimates. (b) Calculated uplift and modeled erosion rates on the central plateau of the island, the same as Figure 7b. (c) Predicted volume fraction of sediment loss from the total erosion. The color scale indicates the probability density function calculated from a thinned ensemble (20%) of the sampled models. Dark blue, light blue, and white bars at the top of the figure indicate the very humid, humid, and semiarid climate settings, respectively, during geological times. Sediment loss ratio is imposed to be invariant within each climate period [Color figure can be viewed at wileyonlinelibrary.com]

(e.g., Cramwinckel et al., 2018; Jenkyns et al., 2004; Pearson et al., 2001) and in southern Africa (Braun et al., 2014; Ponte et al., 2019), as the weathering rate is strongly dependent on the precipitation rate and temperature (e.g., Murphy et al., 2016; White & Blum, 1995). In central and southern Africa, extensive weathering surfaces seem to form during the Cretaceous and Eocene (De Putter & Ruffet, 2020; Guillocheau et al., 2018). In Madagascar, similar planation surfaces with weathering profiles also formed during the early Cenozoic until the Eocene (Delaunay, 2018). For the period since the Pliocene, the modeled high sediment loss ratio could also be a consequence of intense weathering. In the north of Madagascar, a 12 m thick weathering profile is observed at the surface of a late Cenozoic igneous complex (Estrade et al., 2019). In central Africa, the youngest peaks in the age distribution of oxidized manganese ores occur from the late Miocene to the Quaternary. In the modern Congo River basin, the chemical weathering is estimated at 40% of the total budget of erosion (Gaillardet et al., 1995).

Despite the oscillating humidity of the climate model between Oligocene and mid-Miocene (34–11 Ma), our models predict generally

low sediment loss ratios for this period (Figure 11c). The lack of variability in the modeled ratios is primarily due to the coarse temporal resolutions in both sediment volume data and imposed uplift function, and thus cannot be interpreted in further detail regarding the geological or climate histories.

6 | CONCLUSIONS

We have presented a case study that establishes a source-to-sink balance in the sediment volumes between the onshore erosion and offshore sedimentation, based on constraining a landscape evolution model using empirical data. With a focus on the landscape of Madagascar since its separation from India, we modeled the uplift and erosion histories of the island for the past 90 Ma. The uplift function imposed in our models is based on the distribution and heights of the planation surfaces mapped from the island, and the estimated ages of these surfaces. Parameters in the erosion models are either prescribed to commonly used values or constrained by inverse modeling. Data used for constraining the inverse modeling include the cumulative density function of the elevation of the current topography and the incremental volume estimates of sediments from the Morondava Basin off the west coast since the Late Cretaceous. During the inversion, we also examined the potential temporal variation in balance between erosion and sedimentation, by optimizing the ratios of sediment loss for periods of different climate. The results show that the reconciliation between the uplift history and sediment volume data requires a significant fraction of the erosion products being moved out of the source-to-sink system. The models suggest relatively high sediment loss ratios during the warm and humid periods from the Late Cretaceous to the Eocene and from the late Miocene to the present day, implying chemical weathering as an important mechanism for consuming the sediments in regions with no strong tectonic deformation.

ACKNOWLEDGMENTS

Data used in this paper are present in Table 1 and available from Delaunay (2018) [<https://tel.archives-ouvertes.fr/tel-01865476>]. The inverse modeling was performed on the Linux computing clusters at GFZ and PIK. Two anonymous reviewers provided constructive comments and suggestions, which helped improve the paper substantially. Open Access funding enabled and organized by Projekt DEAL.

DATA AVAILABILITY STATEMENT

The data that support the findings of this study are available from the open archive HAL at <https://tel.archives-ouvertes.fr/tel-01865476>.

ORCID

Ruohong Jiao  <https://orcid.org/0000-0003-0303-3118>

REFERENCES

- Bésairie, H. (1973) Précis de géologie malgache. *Annales géologiques de Madagascar*, 36, 142.
- Bertil, D. & Marc Regnault, J. (1998) Seismotectonics of Madagascar. *Tectonophysics*, 294(1-2), 57–74. Available from: [https://doi.org/10.1016/S0040-1951\(98\)00088-2](https://doi.org/10.1016/S0040-1951(98)00088-2)
- Blakey, R.C. (2008) Gondwana paleogeography from assembly to breakup—A 500 m.y. odyssey. In *Resolving the late paleozoic ice age in*

- time and space: *Geological society of america special paper* 441, Fielding, C. R., Frank, T. D. & Isbell, J. L. (eds), Geological Society of America; 1–28. Available from: [https://doi.org/10.1130/2008.2441\(01\)](https://doi.org/10.1130/2008.2441(01))
- Braun, J. (2010) The many surface expressions of mantle dynamics. *Nature Geoscience*, 3(12), 825–833. Available from: <https://doi.org/10.1038/ngeo1020>
- Braun, J. (2018) A review of numerical modeling studies of passive margin escarpments leading to a new analytical expression for the rate of escarpment migration velocity. *Gondwana Research*, 53, 209–224. Available from: <https://doi.org/10.1016/j.gr.2017.04.012>
- Braun, J., Guillocheau, F., Robin, C., Baby, G. & Jelsma, H. (2014) Rapid erosion of the Southern African Plateau as it climbs over a mantle superswell. *Journal of Geophysical Research: Solid Earth*, 119(7), 6093–6112. Available from: <https://doi.org/10.1002/2014JB010998>
- Braun, J., Mercier, J., Guillocheau, F. & Robin, C. (2016) A simple model for regolith formation by chemical weathering. *Journal of Geophysical Research: Earth Surface*, 121(11), 2140–2171. Available from: <https://doi.org/10.1002/2016JF003914>
- Braun, J. & Willett, S.D. (2013) A very efficient O(n), implicit and parallel method to solve the stream power equation governing fluvial incision and landscape evolution. *Geomorphology* 180–181: 170–179. Available from: <https://doi.org/10.1016/j.geomorph.2012.10.008>
- Buerki, S., Devey, D.S., Callmander, M.W., Phillipson, P.B. & Forest, F. (2013) Spatio-temporal history of the endemic genera of Madagascar. *Botanical Journal of the Linnean Society*, 171(2), 304–329. Available from: <https://doi.org/10.1111/boj.12008>
- Celli, N.L., Lebedev, S., Schaeffer, A.J. & Gaina, C. (2020) African cratonic lithosphere carved by mantle plumes. *Nature Communications*, 11(1), 92. Available from: <https://doi.org/10.1038/s41467-019-13871-2>
- Cloetingh, S. & Burov, E. (2011) Lithospheric folding and sedimentary basin evolution: a review and analysis of formation mechanisms. *Basin Research*, 23(3), 257–290. Available from: <https://doi.org/10.1111/j.1365-2117.2010.00490.x>
- Cramwinckel, M.J., Huber, M., Kocken, I.J., Agnini, C., Bijl, P.K., Bohaty, S.M. et al. (2018) Synchronous tropical and polar temperature evolution in the Eocene. *Nature*, 559(7714), 382–386. Available from: <https://doi.org/10.1038/s41586-018-0272-2>
- Cucciniello, C., le Roex, A. P., Jourdan, F., Morra, V., Grifa, C., Franciosi, L. et al. (2018) The mafic alkaline volcanism of SW Madagascar (Ankiloaka, Tulear region): 40 Ar/ 39 Ar ages, geochemistry and tectonic setting. *Journal of the Geological Society*, 175(4), 627–641. Available from: <https://doi.org/10.1144/jgs2017-139>
- Cucciniello, C., Melluso, L., Morra, V., Storey, M., Rocco, I., Franciosi, L. et al. (2011) New 40Ar-39Ar ages and petrogenesis of the Massif d'Ambre volcano, northern Madagascar. In *Volcanism and evolution of the african lithosphere*, Luigi Beccaluva, Gianluca Bianchini, Marjorie Wilson (eds); 257–281. Available from: [https://doi.org/10.1130/2011.2478\(14\)](https://doi.org/10.1130/2011.2478(14))
- Culling, W.E.H. (1960) Analytical Theory of Erosion. *The Journal of Geology*, 68(3), 336–344. <https://doi.org/10.1086/626663>
- Davy, P. & Lague, D. (2009) Fluvial erosion/transport equation of landscape evolution models revisited. *Journal of Geophysical Research: Solid Earth*, 114(3), 1–16. Available from: <https://doi.org/10.1029/2008JF001146>
- De Putter, T. & Ruffet, G. (2020) Supergene manganese ore records 75 Myr-long Campanian to Pleistocene geodynamic evolution and weathering history of the Central African Great Lakes Region - Tectonics drives, climate assists. *Gondwana Research*, 83, 96–117. Available from: <https://doi.org/10.1016/j.gr.2020.01.021>
- de Wit, M.J. (2003) MADAGASCAR: Heads It's a Continent, Tails It's an Island. *Annual Review of Earth and Planetary Sciences*, 31(1), 213–248.
- Delanay, A. (2018) Les mouvements verticaux de Madagascar (90-0 Ma): une analyse couplée des formes du relief et de l'enregistrement sédimentaire des marges ouest malgaches. Ph.D. Thesis.
- Dixey, F. (1960) The geology and geomorphology of Madagascar, and a comparison with Eastern Africa. *Quarterly Journal of the Geological Society*, 116(1–4), 255–268. Available from: <https://doi.org/10.1144/gsjgs.116.1.0255>
- Dohrenwend, J.C. & Parsons A.J. (2009) Pediments in Arid Environments. In *Geomorphology of desert environments*, Springer Netherlands: Dordrecht; 377–411. Available from: https://doi.org/10.1007/978-1-4020-5719-9_13
- Ebinger, C.J. & Sleep, N.H. (1998) Cenozoic magmatism throughout east Africa resulting from impact of a single plume. *Nature*, 395(6704), 788–791. <https://doi.org/10.1038/27417>
- Emerick, C.M. & Duncan, R.A. (1982) Age progressive volcanism in the Comores Archipelago, western Indian Ocean and implications for Somali plate tectonics. *Earth and Planetary Science Letters*, 60(3), 415–428. Available from: [https://doi.org/10.1016/0012-821X\(82\)90077-2](https://doi.org/10.1016/0012-821X(82)90077-2)
- Emmel, B., Boger, S.D., Jacobs, J. & Daszinnies, M.C. (2012) Maturity of central Madagascar's landscape – Low-temperature thermochronological constraints. *Gondwana Research*, 21(2–3), 704–713. Available from: <https://doi.org/10.1016/j.gr.2011.05.018>
- Emmel, B., Jöns, N., Kröner, A., Jacobs, J., Wartho, J.A., Schenk, V. et al. (2008) From Closure of the Mozambique Ocean to Gondwana Breakup: New Evidence from Geochronological Data of the Vohibory Terrane, Southwest Madagascar. *The Journal of Geology*, 116(1), 21–38. Available from: <https://doi.org/10.1086/524121>
- Emmel, B., Jacobs, J., Kastowski, M. & Graser, G. (2006) Phanerozoic upper crustal tectono-thermal development of basement rocks from central Madagascar: An integrated fission-track and structural study. *Tectonophysics*, 412(1–2), 61–86. Available from: <https://doi.org/10.1016/j.tecto.2005.09.008>
- Estrade, G., Marquis, E., Smith, M., Goodenough, K. & Nason, P. (2019) REE concentration processes in ion adsorption deposits: Evidence from the Ambohimirahavavy alkaline complex in Madagascar. *Ore Geology Reviews*, 112, 103027. Available from: <https://doi.org/10.1016/j.oregeorev.2019.103027>
- Gaillardet, J., Dupré, B. & Allègre, C.J. (1995) A global geochemical mass budget applied to the Congo basin rivers: Erosion rates and continental crust composition. *Geochimica et Cosmochimica Acta*, 59(17), 3469–3485. Available from: [https://doi.org/10.1016/0016-7037\(95\)00230-W](https://doi.org/10.1016/0016-7037(95)00230-W)
- Gaillardet, J., Dupré, B., Louvat, P. & Allègre, C.J. (1999) Global silicate weathering and CO₂ consumption rates deduced from the chemistry of large rivers. *Chemical Geology*, 159(1–4), 3–30. Available from: [https://doi.org/10.1016/S0009-2541\(99\)00031-5](https://doi.org/10.1016/S0009-2541(99)00031-5)
- Gallagher, K. (2012) Transdimensional inverse thermal history modeling for quantitative thermochronology. *Journal of Geophysical Research: Solid Earth*, 117(2), B02408. Available from: <https://doi.org/10.1029/2011JB008825>
- Geiger, M., Clark, D.N. & Mette, W. (2004) Reappraisal of the timing of the breakup of Gondwana based on sedimentological and seismic evidence from the Morondava Basin, Madagascar. *Journal of African Earth Sciences*, 38(4), 363–381. Available from: <https://doi.org/10.1016/J.JAFREARSCI.2004.02.003>
- Geiger, M. & Schweigert, G. (2006) Toarcian–Kimmeridgian depositional cycles of the south-western Morondava Basin along the rifted continental margin of Madagascar. *Facies*, 52(1), 85. Available from: <https://doi.org/10.1007/s10347-005-0039-8>
- Grimison, N.L. & Chen, W.-P. (1988) Earthquakes in the Davie Ridge-Madagascar region and the southern Nubian-Somalian plate boundary. *Journal of Geophysical Research: Solid Earth*, 93(B9), 10439–10450. Available from: <https://doi.org/10.1029/JB093iB09p10439>
- Guillocheau, F., Simon, B., Baby, G., Bessin, P., Robin, C. & Dauteuil, O. (2018) Planation surfaces as a record of mantle dynamics: The case example of Africa. *Gondwana Research*, 53, 82–98. Available from: <https://doi.org/10.1016/j.gr.2017.05.015>
- Horner-Johnson, B.C., Gordon, R.G. & Argus, D.F. (2007) Plate kinematic evidence for the existence of a distinct plate between the Nubian and Somalian plates along the Southwest Indian Ridge. *Journal of Geophysical Research*, 112(B5), B05418. Available from: <https://doi.org/10.1029/2006JB004519>

- Howard, A.D. (1994) A detachment-limited model of drainage basin evolution. *Water Resources Research*, 30(7), 2261–2285. Available from: <https://doi.org/10.1029/94WR00757>
- Jenkyns, H.C., Forster, A., Schouten, S. & Sinninghe Damsté, J. S. (2004) High temperatures in the Late Cretaceous Arctic Ocean. *Nature*, 432(7019), 888–892. Available from: <https://doi.org/10.1038/nature03143>
- Jöns, N., Emmel, B., Schenk, V. & Razakamanana, T. (2009) From orogenesis to passive margin – the cooling history of the Bemarivo Belt (N Madagascar), a multi-thermochronometer approach. *Gondwana Research*, 16(1), 72–81. Available from: <https://doi.org/10.1016/J.GR.2009.02.006>
- King, L.C. (1953) Canons of landscape evolution. *Bulletin of the Geological Society of America*, 64(7), 721–752. Available from: [https://doi.org/10.1130/0016-7606\(1953\)64\[721:COLE\]2.0.CO;2](https://doi.org/10.1130/0016-7606(1953)64[721:COLE]2.0.CO;2)
- Kusky, T.M., Toraman, E., Raharimahefa, T. & Rasozanamparany, C. (2010) Active tectonics of the Alaotra–Ankay Graben System, Madagascar: Possible extension of Somalian–African diffusive plate boundary? *Gondwana Research*, 18(2–3), 274–294. Available from: <https://doi.org/10.1016/j.jgr.2010.02.003>
- Mahanjane, E.S. (2014) The Davie Fracture Zone and adjacent basins in the offshore Mozambique Margin—A new insights for the hydrocarbon potential. *Marine and Petroleum Geology*, 57, 561–571. Available from: <https://doi.org/10.1016/J.MARPETGEO.2014.06.015>
- Marquínez, X., Lohmann, L.G., Salatino, M. L. F., Salatino, A. & González, F. (2009) Generic relationships and dating of lineages in Winteraceae based on nuclear (ITS) and plastid (rpS16 and psbA-trnH) sequence data. *Molecular Phylogenetics and Evolution*, 53(2), 435–449. Available from: <https://doi.org/10.1016/j.ympev.2009.07.001>
- Murphy, B.P., Johnson, J. P. L., Gasparini, N.M. & Sklar, L.S. (2016) Chemical weathering as a mechanism for the climatic control of bedrock river incision. *Nature*, 532(7598), 223–227. Available from: <https://doi.org/10.1038/nature17449>
- Nougier, J., Cantagrel, J.M. & Karche, J.P. (1986) The Comores archipelago in the western Indian Ocean: volcanology, geochronology and geodynamic setting. *Journal of African Earth Sciences* (1983), 5(2), 135–145. Available from: [https://doi.org/10.1016/0899-5362\(86\)90003-5](https://doi.org/10.1016/0899-5362(86)90003-5)
- Ohba, M., Samonds, K.E., LaFleur, M., Ali, J.R. & Godfrey, L.R. (2016) Madagascar's climate at the K/P boundary and its impact on the island's biotic suite. *Palaeogeography, Palaeoclimatology, Palaeoecology*, 441, 688–695. Available from: <https://doi.org/10.1016/j.palaeo.2015.10.028>
- Orme, A.R. (2013) 1.12 Denudation, Planation, and Cyclicity: Myths, Models, and Reality. *Treatise on Geomorphology*: 205–232. Available from: <https://doi.org/10.1016/B978-0-12-374739-6.00012-9>
- Peaceman, D.W. & Rachford, J. H. H. (1955) The Numerical Solution of Parabolic and Elliptic Differential Equations. *Journal of the Society for Industrial and Applied Mathematics*, 3(1), 28–41. Available from: <https://doi.org/10.1137/0103003>
- Pearson, P.N., Ditchfield, P.W., Singano, J., Harcourt-Brown, K.G., Nicholas, C.J., Olsson, R.K. et al. (2001) Warm tropical sea surface temperatures in the Late Cretaceous and Eocene epochs. *Nature*, 413(6855), 481–487. Available from: <https://doi.org/10.1038/35097000>
- Piqué, A., Laville, E., Bignot, G., Rabarimanana, M. & Thouin, C. (1999) The initiation and development of the Morondava Basin Madagascar from the Late Carboniferous to the Middle Jurassic: sedimentary, palaeontological and structural data. *Journal of African Earth Sciences*, 28(4), 931–948. Available from: [https://doi.org/10.1016/S0899-5362\(99\)00070-6](https://doi.org/10.1016/S0899-5362(99)00070-6)
- Ponte, J.P., Robin, C., Guillocheau, F., Popescu, S., Suc, J.P., Dall'Asta, M. et al. (2019) The Zambezi delta (Mozambique channel, East Africa): High resolution dating combining bio-orbital and seismic stratigraphies to determine climate (palaeoprecipitation) and tectonic controls on a passive margin. *Marine and Petroleum Geology*, 105, 293–312. Available from: <https://doi.org/10.1016/j.marpetgeo.2018.07.017>
- Pratt, M.J., Wyssession, M.E., Aleqabi, G., Wiens, D.A., Nyblade, A.A., Shore, P. et al. (2017) Shear velocity structure of the crust and upper mantle of Madagascar derived from surface wave tomography. *Earth and Planetary Science Letters*, 458, 405–417. Available from: <https://doi.org/10.1016/j.epsl.2016.10.041>
- Rindrahariasona, E.J., Guidarelli, M., Aoudia, A. & Rambolamanana, G. (2013) Earth structure and instrumental seismicity of Madagascar: Implications on the seismotectonics. *Tectonophysics*, 594, 165–181. Available from: <https://doi.org/10.1016/J.TECTO.2013.03.033>
- Roberts, G.G., Paul, J.D., White, N. & Winterbourne, J. (2012) Temporal and spatial evolution of dynamic support from river profiles: A framework for Madagascar. *Geochemistry, Geophysics, Geosystems*, 13(4), Q04004. Available from: <https://doi.org/10.1029/2012GC004040>
- Roig, J.Y., Tucker, R.D., Peters, S.G., Delor, C. & Theveniaut, H. (2012) Carte Géologique de la République de Madagascar à 1/1,000,000.
- Rouby, D., Bonnet, S., Guillocheau, F., Gallagher, K., Robin, C., Biancotto, F. et al. (2009) Sediment supply to the Orange sedimentary system over the last 150 My: An evaluation from sedimentation/denudation balance. *Marine and Petroleum Geology*, 26(6), 782–794. Available from: <https://doi.org/10.1016/j.marpetgeo.2008.08.004>
- Rowley, D.B. & Garzione, C.N. (2007) Stable Isotope-Based Paleoclimatology. *Annual Review of Earth and Planetary Sciences*, 35(1), 463–508. Available from: <https://doi.org/10.1146/annurev.earth.35.031306.140155>
- Sadler, P.M. (1981) Sediment Accumulation Rates and the Completeness of Stratigraphic Sections. *The Journal of Geology*, 89(5), 569–584. Available from: <https://doi.org/10.1086/628623>
- Sambridge, M. (1999) Geophysical inversion with a neighbourhood algorithm—I. Searching a parameter space. *Geophysical Journal International*, 138(2), 479–494. Available from: <https://doi.org/10.1046/j.1365-246X.1999.00876.x>
- Saria, E., Calais, E., Stamps, D.S., Delvaux, D. & Hartnady, C. J. H. (2014) Present-day kinematics of the East African Rift. *Journal of Geophysical Research: Solid Earth*, 119(4), 3584–3600. Available from: <https://doi.org/10.1002/2013JB010901>
- Seward, D., Grujic, D. & Schreurs, G. (2004) An insight into the breakup of Gondwana: Identifying events through low-temperature thermochronology from the basement rocks of Madagascar. *Tectonics* 23(3). <https://doi.org/10.1029/2003TC001556>
- Stamps, D.S., Kreemer, C., Fernandes, R., Rajaonarison, T.A. & Rambolamanana, G. (2021) Redefining East African Rift System kinematics. *Geology*, 49(2), 150–155. Available from: <https://doi.org/10.1130/G47985.1>
- Stamps, D.S., Saria, E. & Kreemer, C. (2018) A Geodetic Strain Rate Model for the East African Rift System. *Scientific Reports*, 8(1), 732. Available from: <https://doi.org/10.1038/s41598-017-19097-w>
- Stanley, J.R., Braun, J., Baby, G., Guillocheau, F., Robin, C., Flowers, R.M. et al. (2021) Constraining Plateau Uplift in Southern Africa by Combining Thermochronology, Sediment Flux, Topography, and Landscape Evolution Modeling. *Journal of Geophysical Research: Solid Earth* 126(7). Available from: <https://doi.org/10.1029/2020JB021243>
- Stephenson, S.N., White, N.J., Carter, A., Seward, D., Ball, P.W. & Klöcking, M. (2021) Cenozoic Dynamic Topography of Madagascar. *Geochemistry, Geophysics, Geosystems* 22(6). Available from: <https://doi.org/10.1029/2020GC009624>
- Stephenson, S.N., White, N.J., Li, T. & Robinson, L.F. (2019) Disentangling interglacial sea level and global dynamic topography: Analysis of Madagascar. *Earth and Planetary Science Letters*, 519, 61–69. Available from: <https://doi.org/10.1016/j.epsl.2019.04.029>
- Storey, M., Mahoney, J.J., Saunders, A.D., Duncan, R.A., Kelley, S.P. & Coffin, M.F. (1995) Timing of hot spot-related volcanism and the breakup of Madagascar and India. *Science*, 267(5199), 852–855. Available from: <https://doi.org/10.1126/science.267.5199.852>
- Tinker, J., de Wit, M. & Brown, R. (2008) Linking source and sink: Evaluating the balance between onshore erosion and offshore sediment accumulation since Gondwana break-up, South Africa. *Tectonophysics*, 455(1–4), 94–103. Available from: <https://doi.org/10.1016/j.tecto.2007.11.040>
- Torsvik, T.H., Tucker, R.D., Ashwal, L.D., Eide, E.A., Rakotosolof, N.A. & de Wit, M.J. (1998) Late Cretaceous magmatism in Madagascar:

- palaeomagnetic evidence for a stationary Marion hotspot. *Earth and Planetary Science Letters*, 164(1-2), 221–232. Available from: [https://doi.org/10.1016/S0012-821X\(98\)00206-4](https://doi.org/10.1016/S0012-821X(98)00206-4)
- Twidale, C.R. (2002) The two-stage concept of landform and landscape development involving etching: origin, development and implications of an idea. *Earth-Science Reviews*, 57(1-2), 37–74. Available from: [https://doi.org/10.1016/S0012-8252\(01\)00059-9](https://doi.org/10.1016/S0012-8252(01)00059-9)
- van Hinsbergen, D. J. J., de Groot, L.V., van Schaik, S. J., Spakman, W., Bijl, P.K., Sluijs, A. et al. (2015) A paleolatitude calculator for paleoclimate studies. *PLoS ONE*, 10(6), e0126946. Available from: <https://doi.org/10.1371/journal.pone.0126946>
- Wang, Y., Willett, S.D., Wu, D., Haghipour, N. & Christl, M. (2021) Retreat of the Great Escarpment of Madagascar From Geomorphic Analysis and Cosmogenic ¹⁰Be Concentrations. *Geochemistry, Geophysics, Geosystems* 22(12), e2021GC009979. Available from: <https://doi.org/10.1029/2021GC009979>
- Wells, N.A. (2003) Some Hypotheses on the Mesozoic and Cenozoic Paleoenvironmental History of Madagascar. In *The natural history of Madagascar*, Goodman S., Banstead J. (eds), University of Chicago Press: Chicago; 16–34.
- Wescott, W.A. & Diggins, J.N. (1997) Depositional history and stratigraphical evolution of the Sakoa Group (Lower Karoo Supergroup) in the southern Morondava Basin, Madagascar. *Journal of African Earth Sciences*, 24(4), 585–601. Available from: [https://doi.org/10.1016/S0899-5362\(97\)00082-1](https://doi.org/10.1016/S0899-5362(97)00082-1)
- Wescott, W.A. & Diggins, J.N. (1998) Depositional history and stratigraphical evolution of the Sakamena group (Middle Karoo Supergroup) in the southern Morondava Basin, Madagascar. *Journal of African Earth Sciences*, 27(3-4), 461–479. Available from: [https://doi.org/10.1016/S0899-5362\(98\)00073-6](https://doi.org/10.1016/S0899-5362(98)00073-6)
- Whipple, K.X. & Tucker, G.E. (1999) Dynamics of the stream-power river incision model: Implications for height limits of mountain ranges, landscape response timescales, and research needs. *Journal of Geophysical Research: Solid Earth*, 104(B8), 17661–17674. Available from: <https://doi.org/10.1029/1999JB900120>
- White, A.F. & Blum, A.E. (1995) Effects of climate on chemical weathering in watersheds. *Geochimica et Cosmochimica Acta*, 59(9), 1729–1747. Available from: [https://doi.org/10.1016/0016-7037\(95\)00078-E](https://doi.org/10.1016/0016-7037(95)00078-E)
- Yang, R., Willett, S.D. & Goren, L. (2015) In situ low-relief landscape formation as a result of river network disruption. *Nature*, 520(7548), 526–529. Available from: <https://doi.org/10.1038/nature14354>
- Yuan, X.P., Braun, J., Guerit, L., Rouby, D. & Cordonnier, G. (2019) A New Efficient Method to Solve the Stream Power Law Model Taking Into Account Sediment Deposition. *Journal of Geophysical Research: Earth Surface*, 124(6), 1346–1365. Available from: <https://doi.org/10.1029/2018JF004867>
- Zhang, P., Molnar, P. & Downs, W.R. (2001) Increased sedimentation rates and grain sizes 2–4 Myr ago due to the influence of climate change on erosion rates. *Nature*, 410(6831), 891–897. Available from: <https://doi.org/10.1038/35073504>
- Zhuang, G., Zhang, Y.G., Hourigan, J., Ritts, B., Hren, M., Hou, M. et al. (2019) Microbial and Geochronologic Constraints on the Neogene Paleotopography of Northern Tibetan Plateau. *Geophysical Research Letters*, 46(3), 1312–1319. Available from: <https://doi.org/10.1029/2018GL081505>

How to cite this article: Jiao, R., Braun, J., Delaunay, A., Robin, C. & Guillocheau, F. (2023) Linking uplift, erosion, and sedimentation using landscape evolution models: Madagascar since the Late Cretaceous. *Earth Surface Processes and Landforms*, 48(1), 215–229. Available from: <https://doi.org/10.1002/esp.5482>